

Band excitation Kelvin probe force microscopy utilizing photothermal excitation

Liam Collins, Stephen Jesse, Nina Balke, Brian J. Rodriguez, Sergei Kalinin, and Qian Li

Citation: [Applied Physics Letters](#) **106**, 104102 (2015); doi: 10.1063/1.4913910

View online: <http://dx.doi.org/10.1063/1.4913910>

View Table of Contents: <http://scitation.aip.org/content/aip/journal/apl/106/10?ver=pdfcov>

Published by the [AIP Publishing](#)

Articles you may be interested in

[Dual harmonic Kelvin probe force microscopy at the graphene–liquid interface](#)

Appl. Phys. Lett. **104**, 133103 (2014); 10.1063/1.4870074

[The importance of cantilever dynamics in the interpretation of Kelvin probe force microscopy](#)

J. Appl. Phys. **112**, 064510 (2012); 10.1063/1.4754313

[Frequency dependent Kelvin probe force microscopy on silicon surfaces](#)

J. Vac. Sci. Technol. B **27**, 969 (2009); 10.1116/1.3039682

[Kelvin probe force microscopy as a tool for characterizing chemical sensors](#)

Appl. Phys. Lett. **85**, 3926 (2004); 10.1063/1.1810209

[Probing electron charging in nanocrystalline Si dots using Kelvin probe force microscopy](#)

Appl. Phys. Lett. **85**, 3262 (2004); 10.1063/1.1804250

The advertisement features a photograph of the Model PS-100 cryogenic probe station, which is a complex piece of scientific equipment with various mechanical components and a probe. The background is a gradient of blue. The text is arranged around the image: the model name and description on the left, the company logo and name on the right, and a slogan at the bottom right.

Model PS-100
Tabletop Cryogenic
Probe Station

The logo for Lake Shore Cryotronics consists of a stylized blue and white square icon to the left of the company name 'Lake Shore CRYOTRONICS' in a white, sans-serif font.

*An affordable solution for
a wide range of research*

Band excitation Kelvin probe force microscopy utilizing photothermal excitation

Liam Collins,^{1,2,a)} Stephen Jesse,³ Nina Balke,³ Brian J. Rodriguez,^{1,2} Sergei Kalinin,³ and Qian Li^{3,a)}

¹*School of Physics, University College Dublin, Belfield, Dublin 4, Ireland*

²*Conway Institute of Biomolecular and Biomedical Research, University College Dublin, Belfield, Dublin 4, Ireland*

³*Center for Nanophase Materials Sciences, Oak Ridge National Laboratory, Oak Ridge, Tennessee 37831, USA*

(Received 8 February 2015; accepted 19 February 2015; published online 13 March 2015)

A multifrequency open loop Kelvin probe force microscopy (KPFM) approach utilizing photothermal as opposed to electrical excitation is developed. Photothermal band excitation (PthBE)-KPFM is implemented here in a grid mode on a model test sample comprising a metal-insulator junction with local charge-patterned regions. Unlike the previously described open loop BE-KPFM, which relies on capacitive actuation of the cantilever, photothermal actuation is shown to be highly sensitive to the electrostatic force gradient even at biases close to the contact potential difference (CPD). PthBE-KPFM is further shown to provide a more localized measurement of true CPD in comparison to the gold standard ambient KPFM approach, amplitude modulated KPFM. Finally, PthBE-KPFM data contain information relating to local dielectric properties and electronic dissipation between tip and sample unattainable using conventional single frequency KPFM approaches. © 2015 AIP Publishing LLC. [<http://dx.doi.org/10.1063/1.4913910>]

Since its inception in 1991,¹ Kelvin probe force microscopy (KPFM) has had extraordinary success studying local electrochemical,^{2,3} electronic,^{4,5} and transport properties^{6–8} of materials and devices with nanometer resolution. KPFM has been particularly useful for characterizing materials and devices ranging from metals,¹ semiconductors,^{8,9} and ferroelectrics,^{10,11} to self-assembled monolayers,¹² polymers,¹³ and biomolecules.^{14,15} The continued success of KPFM necessitates both the advancement of the technique in terms of accuracy and resolution^{16,17} across all imaging environments,^{18,19} as well as improved capabilities to distinguish and correlate different electronic parameters (i.e., dielectric properties,^{20–23} dissipation^{24,25}) beyond that currently attainable with conventional KPFM.

Although several KPFM “modes” or techniques have been developed,²⁶ most are based on a closed loop bias feedback approach, where an AC voltage (V_{ac}) is applied to a conductive probe such that $V_{probe} = (V_{dc} + V_{cpd}) + V_{ac} \cos(\omega t)$, where V_{cpd} is the built-in contact potential difference (CPD) between tip and sample and V_{dc} is the DC bias controlled by a feedback loop. The driving frequency ω is typically chosen to be close to the cantilever resonance frequency (ω_0) to achieve an amplified cantilever response and hence increased signal to noise ratio. The periodic voltage results in static and dynamic electrostatic forces acting on the tip

$$F_{dc} = -C'_z \left(\frac{1}{2} (V_{dc} - V_{cpd})^2 + \frac{1}{4} V_{ac}^2 \right), \quad (1a)$$

$$F_{\omega} = -C'_z (V_{dc} - V_{cpd}) V_{ac} \sin(\omega t), \quad (1b)$$

$$F_{2\omega} = C'_z \frac{1}{4} V_{ac}^2 \cos(2\omega t), \quad (1c)$$

where C'_z is the capacitance gradient. In amplitude modulation (AM)-KPFM, a lock-in amplifier (LIA) is employed to extract the amplitude ($A(\omega)$) and phase ($\varphi(\omega)$) response due to the first harmonic force, Eq. 1(b), at the frequency of electrical excitation. The mixed amplitude response ($A(\omega) \cos(\varphi(\omega))$) is used as an input to the feedback loop, which works to continually minimize the response (i.e., $F(\omega) = 0$) by adjusting V_{dc} to equal V_{cpd} between the probe and the sample. Assuming ideal KPFM operation, a map of V_{cpd} at each point on the surface can be obtained, however, KPFM closed loop bias feedback is regarded as being non-ideal.^{11,27–29} At best the amplitude response due to $F(\omega)$ can be minimized to the noise level of the system. Furthermore, CPD values measured by KPFM have been shown to be strongly dependent on experimental parameters including V_{ac} ,^{27,30} the operational distance,³¹ and, more worryingly, topographical crosstalk.^{29,32} These parameters can result in systematic errors of hundreds of millivolts in the recorded V_{cpd} , in an instrument specific way, making comparison between experiments or with theory difficult.^{27,28} Several attempts to negate these artifacts present in conventional KPFM have been pursued through the development of KPFM techniques based on heterodyne detection,¹⁷ dual harmonic detection in open^{27,33} and closed loop,³⁴ as well as band excitation (BE)-KPFM.^{29,35}

Another significant problem in AM-KPFM measurements is stray capacitive coupling between different parts of the probe architecture and sample surface under test, which limits the achievable resolution of KPFM measurements. Not only is the conductive tip apex electrostatically interacting with the sample, but the probe cone and cantilever are

^{a)}Authors to whom correspondence should be addressed. Electronic addresses: Liam.Collins@ucdconnect.ie and liq1@ORNL.gov

also influencing the imaging mechanism over a larger sample area.³⁶ Therefore, an AM-KPFM image can be regarded as a weighted average of the CPD across the sample surface and is not solely indicative of the area directly underneath the tip apex. This complication is circumvented to a large degree by frequency modulation (FM)-KPFM,³⁷ which is sensitive to the electrostatic force gradient ($F'(\omega)$) as opposed to the force. The electrostatic force gradient is more sensitive to changes taking place directly under the tip as it decays on much shorter length scales than the electrostatic force and hence is not heavily influenced by the probe cone or cantilever. Note that for the static DC force gradient, F'_{dc} , the cantilever resonance frequency shifts as described by

$$\Delta\omega \approx \omega_0/2k(F'_{dc}), \quad (2a)$$

where k is the cantilever spring constant and

$$F'_{dc} = -C'_z \left(\frac{1}{2} (V_{dc} - V_{cpd})^2 + \frac{1}{4} V_{ac}^2 \right), \quad (2b)$$

where C'_z is the derivative of the capacitance gradient. Although FM-KPFM leads to higher lateral resolution, it is also known to suffer from decreased bias sensitivity compared to AM-KPFM and requires large V_{ac} , which can be problematic when characterizing voltage-sensitive materials.³⁸ Noteworthy, closed loop KPFM techniques only provide a single parameter map of the V_{cpd} , whereas further information on local dielectric properties²⁰⁻²³ or electronic dissipation^{24,25} is attainable using open loop (OL) electrostatic force microscopy (EFM). Recently, BE-KPFM has shown promise in capturing information beyond what is obtainable using conventional KPFM and or EFM alone.^{17,22,34}

In this work, we utilize the BE approach to compare the implementation of different physical actuation mechanisms for multifrequency KPFM, namely, capacitive (i.e., OLBE-KPFM²⁹) and photothermal (i.e., photothermal (Pth)BE-KPFM) actuation. Both approaches operate in open loop, negating complications arising from closed loop bias feedback as well as being sensitive to the electrostatic force gradient overcoming to a large degree the stray capacitance effect. The sensitivity to small changes in the electrostatic force gradient is compared between the newly developed PthBE-KPFM and the previously reported OLBE-KPFM.²⁹

Finally, we compare PthBE-KPFM with the gold standard for surface potential mapping in ambient, namely, AM-KPFM.

BE,³⁹ unlike single frequency detection, allows the full cantilever response to be determined in a frequency band typically comprising the cantilever resonance peak. Combined with open loop KPFM bias spectroscopy, BE can be used to map electronic properties of the sample under test.²⁹ Fig. 1(a) shows a schematic of the setup used in this work. All BE-KPFM techniques shown here are performed on an Asylum Research Cypher platform equipped with a photothermal excitation module (BlueDriveTM) and a home-built BE controller. Measurements were performed with as-received Pt/Ir-coated (Nanosensors, PPP-EFM) AFM probes with a nominal mechanical resonance frequency and spring constant of 75 kHz and 2.8 N/m, respectively. We use a NI PXI-6124 card with two analog outputs to synchronously generate BE and DC waveforms that are digitally constructed from a set of parameters, e.g., bandwidth, amplitude, and pulse length.

Common to both capacitive and photothermal actuation open loop KPFM approaches is the use of DC bias pulses applied directly to the cantilever, used to induce changes in the electrostatic interactions between probe and sample. BE waveforms are used to detect the resultant changes in the dynamic cantilever response by recording the resonance peak of the oscillating cantilever. The difference between OLBE-KPFM²⁹ and PthBE-KPFM is simply where the BE signal is supplied for excitation. In OLBE-KPFM, the BE excitation waveform is applied as a voltage directly to the conductive probe, as shown in Fig. 1. Conversely, in PthBE-KPFM, the BE waveform is used to modulate the photothermal laser module directly, as shown in Fig. 1. In photothermal excitation, the laser modulates the temperature of the cantilever base, resulting in cantilever oscillation based on thermal expansion. PthBE has previously been used to measure bias induced transitions based on short range interactions with the tip held in contact with the sample.⁴⁰ In this work, we describe how a similar methodology applied to KPFM, operated in non-contact, can be used to extract quantitative information on local electrochemical and electronic properties. In the current setup, we perform BE-KPFM in a grid measurement where the tip is moved along a dense grid of points, and at each grid position, the tip is brought into contact to find the sample surface and then immediately

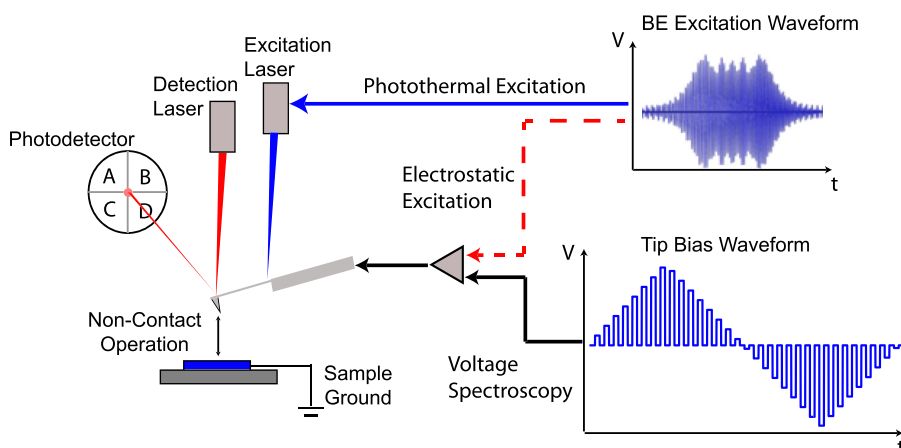


FIG. 1. Schematic of the working principle behind both OLBE (red dashed line) and PthBE (blue line)—KPFM utilizing electrostatic and photothermal excitation of the cantilever, respectively. Modulation of the excitation signal is performed in a band of frequencies comprising the cantilever resonance. Voltage spectroscopy is performed in this case using a DC bipolar square wave applied between a conductive probe and sample.

retracted a defined sample distance (typically 50–200 nm) before voltage modulation begins. On receiving each BE waveform, the cantilever starts to oscillate at the chosen band of frequencies. The time domain responses of the cantilever are acquired over the same time length and then Fourier transformed into frequency domain response spectra, which contain the tip-sample interaction information. The simple harmonic oscillator (SHO) model can accurately describe a free resonance frequency spectrum, which has amplitude/phase forms as

$$A(\omega) = \frac{\omega_0^2 A_{drive}}{\sqrt{(\omega_0^2 - \omega^2)^2 + (\omega_0 \omega / Q)^2}}, \quad (3a)$$

$$\varphi(\omega) = \tan^{-1}\left(\frac{\omega_0 \omega}{Q(\omega_0^2 - \omega^2)}\right) + \varphi_{drive}, \quad (3b)$$

where ω_0 is the resonance frequency and quality (Q) factor; A_{drive} and φ_{drive} are the amplitude and phase, respectively, of the driving force.

Fig. 2 shows comparative measurements between OLBE- and PthBE-KPFM performed sequentially at a distance of 60 nm above an Au electrode. Fig. 2(a) depicts a single point OLBE amplitude spectrum, showing strong variation in the cantilever transfer function as a function of V_{dc} . In the case of OLBE, where the system is capacitively driven, we expect a linear V_{dc} dependence of the amplitude, Fig. 2(c), which becomes nullified at V_{cpd} governed by the first harmonic electrostatic force, Eq. 1(b). Note, linear fitting of this response can be used to determine CPD and capacitance gradient from the nulling bias of the amplitude response and slope, respectively. Additionally, BE allows passive tracking of the resonance frequency, which demonstrates a parabolic bias dependence, as described by the electrostatic force gradient, Eq. 2(b). In this case, the parabola maximum corresponds to the CPD. This KPFM

measurement is expected to have a higher spatial resolution as described previously for FM-KPFM. Note that, from Fig. 2(d), the electrical excitation approach (i.e., OLBE-KPFM) suffers from poor sensitivity at biases approaching the CPD value. The response becomes increasingly smaller approaching the CPD, eventually becomes nullified at precisely V_{cpd} , decreasing the accuracy of the SHO fitting procedure used to determine the resonance frequency. The results of a similar measurement collected using PthBE-KPFM are shown. In PthBE-KPFM, Fig. 2(c), a strong cantilever response is recorded, which is largely independent of applied bias. This is expected from photothermal excitation as it is more insensitive to long range electrostatic force than OLBE-KPFM. PthBE-KPFM is, however, highly sensitive to the electrostatic force gradient as evident from the change in resonance frequency shown in Fig. 2(d), and is shown to be more sensitive to small changes in the resonance frequency at bias values close to the CPD in comparison to OLBE-KPFM.

To illustrate PthBE-KPFM imaging, we have chosen a model sample combining topographic, material, and charge contrast, as shown in Fig. 3. Fig. 3(a) shows the AFM topography of the test sample formed by an Au electrode deposited on a Si surface with a native oxide, having a step of about 150 nm of height. A positive charge region is written on the SiO_x surface using bias lithography by scanning a tip biased with 9 V in contact mode using a scan rate of 0.5 Hz in an area of $1.5 \mu\text{m}^2$ indicated in Fig. 3(a). Measurements were first performed using classical KPFM operated in lift mode (lift height = 50 nm) using AM detection. In AM-KPFM, Fig. 3(b), a CPD of $502 \pm 18 \text{ mV}$ and $202 \pm 9 \text{ mV}$ was found for SiO_x and Au, respectively. The CPD of the charged SiO_x region increased by approximately 351 mV to $853 \pm 19 \text{ mV}$ in comparison to uncharged SiO_x . In general, it is clear that the charged region observed using AM-KPFM (Fig. 3(b)) is much more diffuse than the physically charged region indicated in Fig. 3(a), likely a consequence of the

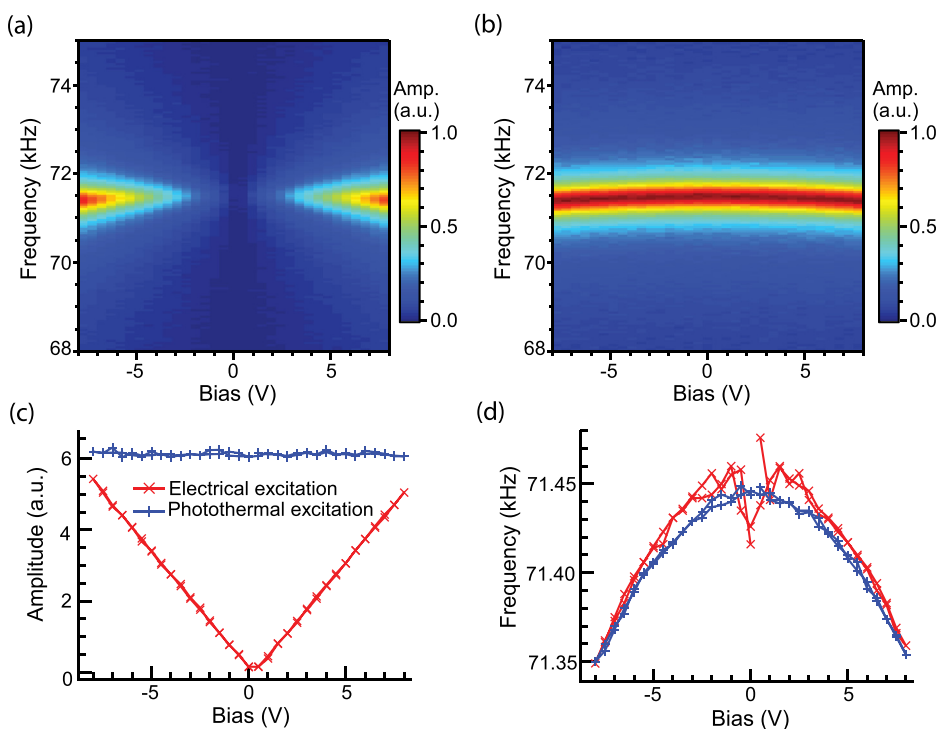


FIG. 2. Single-pixel cantilever response amplitude versus bias and frequency acquired at one location on Au/ SiO_x using (a) OLBE-KPFM and (b) PthBE-KPFM, respectively. Bias dependence of (c) cantilever response amplitude and (d) resonant frequency for OLBE (red line) and PthBE (blue line)—KPFM, respectively. Linear fit of the bias dependence of the cantilever response gives rise to capacitance gradient (slope) and CPD (nulling bias). Parabolic fitting of the bias dependence of the frequency response gives second derivative capacitance gradient (slope) and CPD (bias maxima).

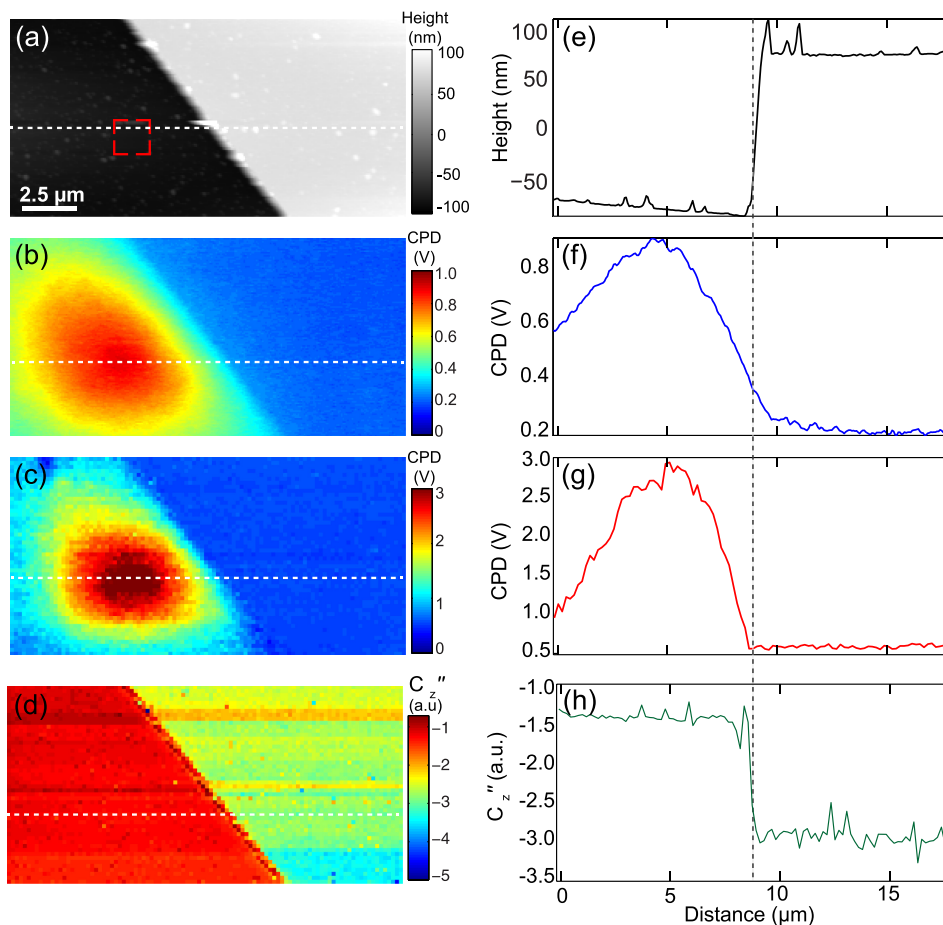


FIG. 3. (a) AFM topography image collected in tapping mode across a SiO_x/Au boundary collected after charging a $2\ \mu\text{m}$ area of SiO_x as indicated with the dashed red box. KPFM maps of the CPD collected using (b) standard AM-KPFM (lift height = 50 nm) and (c) PthBE-KPFM (lift height = 50 nm) and (d) C''_z obtained from PthBE-KPFM data. (g) and (h) Corresponding cross sections taking from areas indicated by dashed white lines in (a)–(d), respectively.

long range nature of the electrostatic force interaction. Next, the same area was measured using PthBE-KPFM across a 100×50 grid using a BE excitation of 250 mV centered at 72 kHz having a bandwidth of 20 kHz and 129 bins per band. The DC bias waveform was within the range of ± 8 V having 64 steps per waveform. The CPD was calculated for each position by parabolic fitting of the bias dependence of the resonance frequency. In PthBE-KPFM, Fig. 3(c), a CPD of 945 ± 16 mV and 560 ± 5 mV was found for SiO_x and Au, respectively. PthBE-KPFM shows a higher CPD (2.18 ± 0.03 V) and represents a more localized measurement of the true CPD of the charge region than observed using standard AM-KPFM, likely due to detection of the

electrostatic force gradient, which is localized to the last few nanometers of the tip apex. Note that information on the dielectric properties is also determined from the fitting procedure, providing the C''_z as shown in Fig. 3(d). Clear contrast in material properties between SiO_x and Au can be observed in the C''_z map, having a sharp transition region at the boundary. Furthermore, no indications of variation in dielectric constant in the charged region are observed, suggesting the dielectric constant remains constant in this region, in agreement with the absence of an oxide layer growth in the topography image. From the line scan analysis (Figs. 3(e)–3(h)), it is clear that the PthBE method, even operated in grid mode having less sampling pixels, shows

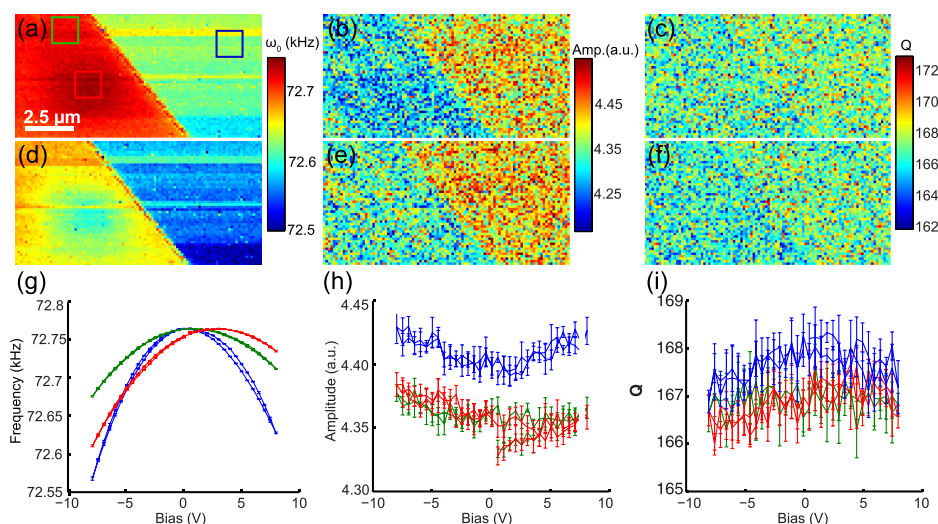


FIG. 4. (a) and (d) Resonance frequency, (b) and (e) amplitude, (c) and (f) and Q factor recorded using PthBE-KPFM at (a)–(c) positive 8 V and (d)–(f) negative 8 V, respectively. Bias dependence of the (g) resonance frequency, (h) amplitude, and (i) Q factor from (green) uncharged SiO_x (red) charged SiO_x and (blue) Au.

intrinsically much higher lateral resolution than observed using standard AM-KPFM.

In addition to providing a more localized CPD measurement, PthBE-KPFM provides information on all the cantilever SHO parameters and their local variation across the sample surface. Furthermore, the bias-dependence of cantilever dynamics can provide additional material-specific information. For example, the Q factor of the cantilever contains information on the dissipation processes in tip-surface system.³⁹ In Fig. 4, the resonance frequency, amplitude, and Q factor for +8 and -8 V_{dc} are shown, respectively. There is clear contrast between materials, and between bias voltage points, for the resonance frequency. More subtle changes in the amplitude and Q factor maps can also be observed. It is likely that voltage spectroscopy as used in PthBE-KPFM can uncover dissipative interactions. This is demonstrated in Figs. 4(g)–4(i), which shows the average bias dependence of the SHO parameters for SiO_x , charged SiO_x , and Au. The average peak amplitude and Q factor are higher for Au in comparison to the SiO_x substrate, indicating an increased electrical dissipation on the SiO_x surface. Furthermore, little or no change in the bias dependence of the amplitude or Q factor between charged and uncharged SiO_x is observed, suggesting that the difference is inherently related to the material properties and independent on the magnitude of the response. Note that in OLBE-KPFM, the strong changes of response amplitude with bias render these measurements difficult because of complications in fitting the SHO peak as a result of small amplitude responses.²⁹ However, the relatively strong bias independent amplitude observed using PthBE-KPFM negates this problem.

To summarize, we demonstrate an approach for CPD mapping based on OLBE-KPFM combined with photothermal as opposed to capacitive excitation. PthBE-KPFM produces CPD maps comparable to conventional AM-KPFM but having improved lateral resolution and being a more localized measurement as PthBE-KPFM is sensitive to the electrostatic force gradient. We have explored the use of PthBE-KPFM voltage spectroscopy on a SiO_x/Au test sample, which revealed small but detectable changes in bias dependence of amplitude and Q factor. Such changes appear to be characteristic of variation in electronic dissipation between the electrode and insulating junction, which is unattainable using conventional KPFM. PthBE-KPFM demonstrated here can be easily extended to a scanning mode with speeds comparable to standard KPFM as seen in OLBE-KPFM.²⁹ Furthermore, it is likely that this approach can be extended to liquid environments in the form of electrochemical force microscopy, while avoiding AC induced electrochemistry in liquid present in the existing approach.¹⁹

This research was conducted at the Center for Nanophase Materials Sciences, which is sponsored at Oak Ridge National Laboratory by the Scientific User Facilities Division, Office of Basic Energy Sciences, U.S. DOE. Personal support was provided by the U.S. DOE, Basic Energy Sciences, Materials Sciences and Engineering Division through the Office of Science Early Career Research Program (N.B. and Q.L.).

¹M. Nonnenmacher, M. P. O'Boyle, and H. K. Wickramasinghe, *Appl. Phys. Lett.* **58**(25), 2921–2923 (1991).

- ²D. B. Blücher, J.-E. Svensson, L.-G. Johansson, M. Rohwerder, and M. Stratmann, *J. Electrochem. Soc.* **151**(12), B621–B626 (2004).
- ³V. Guillaumin, P. Schmutz, and G. Frankel, *J. Electrochem. Soc.* **148**(5), B163–B173 (2001).
- ⁴S. Mugo and J. Yuan, *J. Phys.: Conf. Ser.* **371**, 012030 (2012).
- ⁵D. Ziegler, P. Gava, J. Güttinger, F. Molitor, L. Wirtz, M. Lazzeri, A. Saitta, A. Stemmer, F. Mauri, and C. Stampfer, *Phys. Rev. B* **83**(23), 235434 (2011).
- ⁶E. Strelcov, S. Jesse, Y.-L. Huang, Y.-C. Teng, I. I. Kravchenko, Y.-H. Chu, and S. V. Kalinin, *ACS Nano* **7**(8), 6806–6815 (2013).
- ⁷E. Strelcov, Y. Kim, S. Jesse, Y. Cao, I. N. Ivanov, I. I. Kravchenko, C.-H. Wang, Y.-C. Teng, L.-Q. Chen, and Y. H. Chu, *Nano Lett.* **13**(8), 3455–3462 (2013).
- ⁸M. Tanimoto and O. Vatel, *J. Vac. Sci. Technol., B: Microelectron. Nanometer Struct.* **14**(2), 1547–1551 (1996).
- ⁹P. Girard, *Nanotechnology* **12**(4), 485 (2001).
- ¹⁰S. V. Kalinin and D. A. Bonnell, *Phys. Rev. B* **62**(15), 10419 (2000).
- ¹¹S. V. Kalinin and D. A. Bonnell, *Phys. Rev. B* **63**(12), 125411 (2001).
- ¹²J. Lü, L. Eng, R. Bennewitz, E. Meyer, H. J. Güntherodt, E. Delamarche, and L. Scandella, *Surf. Interface Anal.* **27**(5–6), 368–373 (1999).
- ¹³H. Hoppe, T. Glatzel, M. Niggemann, A. Hirsch, M. C. Lux-Steiner, and N. Sariciftci, *Nano Lett.* **5**(2), 269–274 (2005).
- ¹⁴C. Leung, H. Kinns, B. W. Hoogenboom, S. Howorka, and P. Mesquida, *Nano Lett.* **9**(7), 2769–2773 (2009).
- ¹⁵A. K. Sinensky and A. M. Belcher, *Nat. Nanotechnol.* **2**(10), 653–659 (2007).
- ¹⁶U. Zerweck, C. Loppacher, T. Otto, S. Grafström, and L. M. Eng, *Phys. Rev. B* **71**(12), 125424 (2005).
- ¹⁷Y. Sugawara, L. Kou, Z. Ma, T. Kamijo, Y. Naitoh, and Y. J. Li, *Appl. Phys. Lett.* **100**(22), 223104 (2012).
- ¹⁸L. Collins, J. I. Kilpatrick, I. V. Vlasiouk, A. Tselev, S. A. Weber, S. Jesse, S. V. Kalinin, and B. J. Rodriguez, *Appl. Phys. Lett.* **104**(13), 133103 (2014).
- ¹⁹L. Collins, S. Jesse, J. I. Kilpatrick, A. Tselev, O. Varenyk, M. B. Okatan, S. A. Weber, A. Kumar, N. Balke, S. V. Kalinin, and B. Rodriguez, *Nat. Commun.* **5**, 3871 (2014).
- ²⁰L. Fumagalli, D. Esteban-Ferrer, A. Cuervo, J. L. Carrascosa, and G. Gomila, *Nat. Mater.* **11**(9), 808–816 (2012).
- ²¹L. Fumagalli, G. Ferrari, M. Sampietro, and G. Gomila, *Nano Lett.* **9**(4), 1604–1608 (2009).
- ²²L. Fumagalli, G. Gramse, D. Esteban-Ferrer, M. Edwards, and G. Gomila, *Appl. Phys. Lett.* **96**(18), 183107 (2010).
- ²³G. Gramse, I. Casuso, J. Toset, L. Fumagalli, and G. Gomila, *Nanotechnology* **20**(39), 395702 (2009).
- ²⁴W. Denk and D. W. Pohl, *Appl. Phys. Lett.* **59**(17), 2171–2173 (1991).
- ²⁵M. J. Cadenas, R. Misiego, K. C. Smith, A. Avila, B. Pipes, R. Reifengerger, and A. Raman, *Nanotechnology* **24**(13), 135706 (2013).
- ²⁶S. Sadewasser and T. Glatzel, *Kelvin Probe Force Microscopy* (Springer, 2012).
- ²⁷L. Collins, J. Kilpatrick, S. A. Weber, A. Tselev, I. Vlasiouk, I. Ivanov, S. Jesse, S. Kalinin, and B. Rodriguez, *Nanotechnology* **24**(47), 475702 (2013).
- ²⁸T. Mélin, S. Barbet, H. Diesinger, D. Théron, and D. Deresmes, *Rev. Sci. Instrum.* **82**(3), 036101 (2011).
- ²⁹S. Guo, S. V. Kalinin, and S. Jesse, *Nanotechnology* **23**, 125704–125713 (2012).
- ³⁰Y. Wu and M. A. Shannon, *Rev. Sci. Instrum.* **77**, 043711 (2006).
- ³¹A. Liscio, V. Palermo, K. Müllen, and P. Samorì, *J. Phys. Chem. C* **112**(44), 17368–17377 (2008).
- ³²K. Okamoto, Y. Sugawara, and S. Morita, *Appl. Surf. Sci.* **188**(3–4), 381–385 (2002).
- ³³L. Collins, J. Kilpatrick, M. Bhaskaran, S. Sriram, S. Weber, S. Jarvis, and B. Rodriguez, in *Applications of Ferroelectrics Held Jointly with 2012 European Conference on the Applications of Polar Dielectrics and 2012 International Symposium on Piezoresponse Force Microscopy and Nanoscale Phenomena in Polar Materials (ISAF/ECAPD/PFM)* (IEEE, 2012), pp. 1–4.
- ³⁴M. Lee, W. Lee, and F. B. Prinz, *Nanotechnology* **17**(15), 3728 (2006).
- ³⁵S. Guo, S. V. Kalinin, and S. Jesse, *Appl. Phys. Lett.* **100**(6), 063118 (2012).
- ³⁶H. Jacobs, P. Leuchtman, O. Homan, and A. Stemmer, *J. Appl. Phys.* **84**(3), 1168–1173 (1998).
- ³⁷S. I. Kitamura and M. Iwatsuki, *Appl. Phys. Lett.* **72**(24), 3154–3156 (1998).
- ³⁸S. Yoshida, J. Kikuchi, Y. Kanitani, O. Takeuchi, H. Oigawa, and H. Shigekawa, *e-J. Surf. Sci. Nanotechnol.* **4**(0), 192–196 (2006).
- ³⁹S. Jesse, S. V. Kalinin, R. Proksch, A. Baddorf, and B. Rodriguez, *Nanotechnology* **18**(43), 435503 (2007).
- ⁴⁰Q. Li, S. Jesse, A. Tselev, L. Collins, P. Yu, I. Kravchenko, S. V. Kalinin, and N. Balke, *ACS Nano* **9**(2), 1848 (2015).